Vacuum 194 (2021) 110589

Contents lists available at ScienceDirect

Vacuum

journal homepage: www.elsevier.com/locate/vacuum

Growth kinetics analysis of Nb–Al intermetallic compounds interfacial layers based on Nb–Al phase diagram

Xianjun Lei [a,b], Xiaopeng Wang [c,d], Fantao Kong [a,b,*], Haitao Zhou [e], Yuyong Chen [a,b]

[a] State Key Laboratory of Advanced Welding and Joining, Harbin Institute of Technology, Harbin, 150001, China
[b] School of Materials Science and Engineering, Harbin Institute of Technology, Harbin, 150001, China
[c] Center of Analysis and Measurement, Harbin Institute of Technology, Harbin, 150001, China
[d] National Key Laboratory for Precision Hot Processing of Metals, Harbin Institute of Technology, Harbin, 150001, China
[e] Shanghai Spaceflight Precision Machinery Institute, Shanghai, 201600, China

ARTICLE INFO

Keywords:
Niobium aluminides
Diffusion coefficient
Growth kinetics
Intermetallic compound
Phase diagram

ABSTRACT

A model for studying the growth kinetics of intermetallic compounds by means of binary phase diagrams was proposed with some assumptions. The parabolic growth relationship of intermetallic compound is deduced mathematically using analytical solution of diffusion equations and the mass balance law. By comparing the solubility of the adjacent phase in intermetallic compound phase, the predominant parameter controlling the growth kinetics is the solute diffusion coefficient. The diffusion coefficient of Al atoms in intermetallic layers is quantitatively described and the smallest diffusion coefficient is 0.373×10^{-21} m^2/s in Nb_3Al phase. It is demonstrated intermetallic layers formed at interface indeed inhibit the Nb container being corroded further by TiAl melt, and Nb_3Al layer is a dominant factor.

1. Introduction

As a potential structural material, TiAl alloys have become a significant and burgeoning high-temperature application materials in aerospace and aeronautics industry [1], owing to their superior advantages over the conventional superalloys, such as low density, high strength ratio and high stiffness ratio [2]. As of today, the maximum service temperature of TiAl alloys can be to 800 °C, however, the target service temperature hopes up to 900–950 °C in the future [3]. Ti–Al–Nb alloy single crystals had been fabricated and exhibited excellent high temperature and ambient temperature performance [4], indicating a perfect match between room temperature processing and high temperature service potential [5,6]. However, during the fabrication and processing of TiAl alloys [7–14], many metal components suffer from corrosion to different extent triggered by corrosive Al element and its alloy melts on account of high chemical activity and affinity [15]. This corrosion process drastically reduces the service lifetime of TiAl alloys and causes the contamination of TiAl melts, which in turn compromises the efficiency of TiAl alloys processing and product quality. Efficient protection against corrosion has been one of the challenges for the sustainability of industrial facilities. Intermetallic compounds emerge as stable phases at the interface where they can produce a number of effects including changing the interfacial energy, acting as a diffusion barrier and thus mediating further dissolution of the substrate metal, which are important for understanding and controlling corrosion behavior [16,17]. It is necessary to figure out the kinetics of intermetallic compounds growth and how they affect the corrosion courses, as aforementioned, which is desired for development of improving materials and process.

In some cases, technically, growth kinetics were studied by diffusion couples with two pure elements annealing at different temperature for appropriate times, investigating the dynamic behavior of the intermetallic phase and the growth law can be obtained experimentally [18,19]. However, the method generally requires intermetallic layers are relatively thin and morphological clear. Therefore, it is difficult to quantitatively estimate the thickness of the intermetallic compounds layers accurately where the phases boundaries are ambiguous. According to Kidson's opinion [20], not all phases which appear in the phase diagram necessarily observed. Indeed, in certain alloy systems, stable intermetallic compounds layers may not be detected within realistic time at experimental temperature [21]. Else, if there exists a barrier layer at the interface, an equilibrium phase maybe absence, notorious examples are some phases in Sn–Ag–Ni system [22], Ni–Al–Cr system [23] Si–C-X (X: Nb, Ti, Mo) system [24]. Under these circumstances, such consideration will give rise to difficulty for intuitive understanding of the kinetics

* Corresponding author. Room 402, Department of Materials Science and Engineering, Harbin Institute of Technology, No.92 Xidazhi Street, Harbin, 15000, China.
E-mail address: kft@hit.edu.cn (F. Kong).

https://doi.org/10.1016/j.vacuum.2021.110589
Received 17 June 2021; Received in revised form 7 September 2021; Accepted 8 September 2021
Available online 15 September 2021
0042-207X/

process. A analysis kinetics was proposed to understand the diffusion-controlling diffuion process from theoretical aspect in a hypothetical binary system [25], but lack of experimental verification and the relevant details. In some ternary systems, the growth kinetics of intermetallic compound layers are only described by empirical formulas [22,23,26], without the relevant theoretical basis to help understand the influencing factors of the processes. The quantitative relationships cannot be established for kinetics assessment. In these systems, if the growth rate of the relevant intermetallic compounds is not large enough to observe its appearance with realistic experiment. To date, we have not had an effective method to estimate their growth kinetics accurately even though the intermetallic compounds are thermodynamically stable. Therefore, it is imperative to explore a convenient and easy mean to analyze the thickness of the intermetallic compounds layers resonable so as to the growth kinetics can be obtained. For determination of a reliable growth kinetics, using phase diagram rationally and the experimental information on the kinetics assessment is essentially important [27].

On the other hand, the growth kinetics of intermetallic compounds is significantly important for understanding and controlling of intermetallic interaction and corrosion process, which requires a reasonable, simple and economical method to evaluate the interaction process. Under these conditions, an analysis model based on studying the growth kinetics of intermetallic compounds by means of binary phase diagrams was proposed, in which only solute concentration should be taken into account to describe the kinetics of the reactive diffusion mathematically. The present study attempts to elicit the parameters which govern the reaction kinetics for intermetallic layer growth during interdiffusion between Nb container and TiAl melt under interaction process with a special focus on understanding the effects of Al on the interdiffusion and corrosion process. The kinetics of intermetallics compounds layers has been theoretically analyzed based on phase diagram and the mass conservation law, then experimental verification. Experimental and theoratical, the quantitative relationship between intermetallic compounds layers thickness and corrosion time is approximately established and the diffusion coeffection is calculated reasonably. The primary purpose of this study is to figure out the transferring mechanism of Al atoms during the diffusion between high temperature TiAl melt and Nb container and to develop a quantitatively kinetics of intermetallic compounds layers growth in terms of anomalous Al diffuse and corrode into the Nb phase. The additional destination of the present work is to contribute to an increased understanding of the fundamental scientific aspects of interdiffusion and dynamic corrosion. The results represent a basis which should allow engineers to improve process technology.

2. Experiments

The interfacial interaction experiments were performed between Nb containers and Ti–47Al–2Nb(at.%) alloys with different corrosion time at 1600 °C. The cast cylindrical raw ingots with the dimensions of ∅ 40 × 150 mm used in this research were produced using induction skull melting (ISM) with 99.99 wt%Ti, 99.99 wt%Al, Nb–Al alloy under an argon atmosphere. In order to promote homogeneity, the ingots were remelt at least five times. Bars with 8 mm in diameter and 50 mm in length were cut from the ingot center by wire-electrode cutting and removed oxide by standard metallographic techniques, then cleaned ultrasonically in a bath of anhydrous ethanol for 30 min. Each bar was placed into a Nb (99.95 wt%) container (external diameter 12 mm, inner diameter 8 mm, surface finish 1.6) which also cleaned ultrasonically in a bath of anhydrous ethanol for 30 min. The experiments were carried out in the Bridgman type apparatus, the Nb container was fixed in the setup, then the furnace chamber was evacuated at a 5×10^{-3} Pa, and filled with high-purity argon of 0.05 MPa as protection. After heating to 1600 °C and corrosion different times, then quenching quickly. Heat treatment experiments were conducted in a vacuum tube furnace (vacuumed to 5×10^{-3} Pa and back-filled with high purity argon to 0.2 MPa). After the experiments, the solidified bars were sectioned transversely and then polished perpendicular to the interface using standard metallographic techniques to study the interaction layers. A scanning electron microscope (SEM, FEI Quanta 200F) equipped with energy dispersive X-ray spectrometer (EDS) was employed to examine the microstructures and determine the concentrations of Nb, Al and Ti elements as a function of distance across the interaction layer. More than ten different microstructural fields were examined in each sample to determine the thicknesses of reaction layers. The Image J software was employed to measure the thicknesses of intermetallic compound layers formed by the interfacial interaction for quantitatively analysis, and each intermetallic compound layer thickness should take an average of more than 5 measurements.

3. Modeling of corrosion resistance layers growth kinetics

To decrease the dissolution rate of Nb, a better adherence of the natural corrosion products layer of Nb is necessary. Indeed, the natural corrosion products layer on Nb container inner surface can be named corrosion resistance Nb–Al intermetallic layer. According to the previous studies [28–30] and Nb–Al binary phase diagram (Fig. 1(a)), it can be deduced that the intermetallic compounds phases $(Nb,Ti)_2Al$ and $(Nb,Ti)_3Al$ are formed when Nb container interacts with TiAl alloys melt because of Ti element dissolve into Nb–Al intermetallic compounds to form solid solution [31], the maximum solubility of Ti in Nb_3Al is about 20 at.%, as shown in Fig. 1(b) what's more, in Nb-based alloys the concentration of Ti is maintained to about 25 at.% to ensure that the melting temperature of the alloys is above 1700 °C, and Ti provides strong solid solution strengthening (like Al, Cr, Hf, Mo, Ta, and W). As-cast material, the synergy among alloying elements can influence significantly the composition of phase [32]. In the presence of Ti, the solid solubilities of Al increase with increasing Ti concentration in the Nb(BCC) [33,34]. Nevertheless, the structures of $(Nb,Ti)_2Al$ and $(Nb,Ti)_3Al$ are still σ-CrFe($D8_b$) and Cr_3Si(A15), respectively, this appears to be consistent with the notion that low-carbon steel and Al-5wt.%Si alloy [35]. It is concluded that the melting point of Nb_3Al and Nb_2Al changed a little after a small amount of Ti dissolved into them. Therefore, this structure seems to support the idea that the interfacial interaction between Nb container and TiAl alloys melt can be regarded as Al element in TiAl alloys melt interacts with Nb container, and the dominant diffusion mechanism is controlled by the movement of aluminum atoms [36]. In this circumstance, ternary system can be approximated to a binary system to investigate growth kinetics of Nb–Al intermetallic compounds.

The kinetics equation can be derived based on the consumptions as follows:

(1) Growth of the intermetallic compounds layers is controlled only by the diffusion of Al element, the diffusion of Ti in the same direction is negligible,
(2) The solubility of Ti in Nb–Al intermetallic compounds is negligible,
(3) The local equilibrium is established at each migrating interface, the migration of the interface is controlled by the volume diffusion in the neighboring phases,
(4) The diffusion coefficient for the volume diffusion is independent of the composition in each phase.

According to the previous investigation [38], the interaction process between TiAl alloy melt and Nb container was essential course where Al element diffused into the boundary region of Nb container during the erosion to form intermetallic compounds. Therefore, in the binary Nb–Al system, as shown in Fig. 2(a), the intermetallic compounds phase Nb_2Al (the melting point 1870 °C) and $Nb_2Al + Nb_3Al$ are formed but the intermetallic compounds Nb_3Al(the melting point 1960 °C) and the solid solutions $Nb_3Al + Nb$(BCC) after a sufficiently long corrosion time at the temperature T, in other words, to corrode Nb container further, the Al

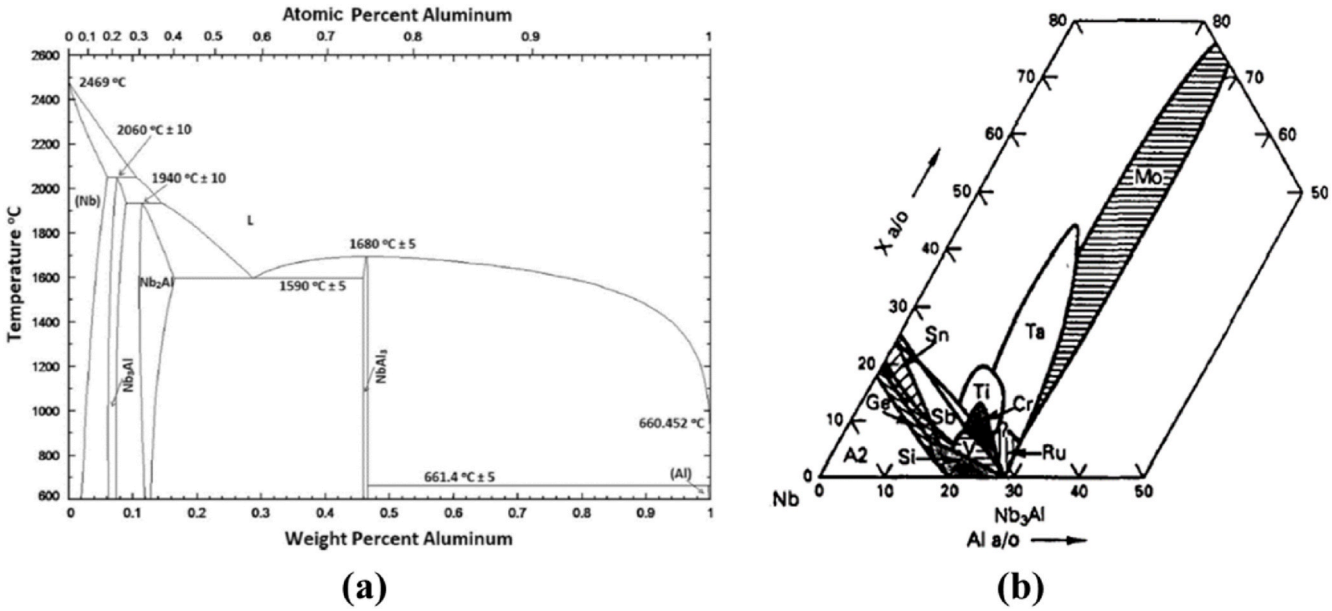

Fig. 1. (a) Binary phase diagram of the Nb–Al system [37], (b) Effect of ternary additions on the Nb_3Al phase field [31].

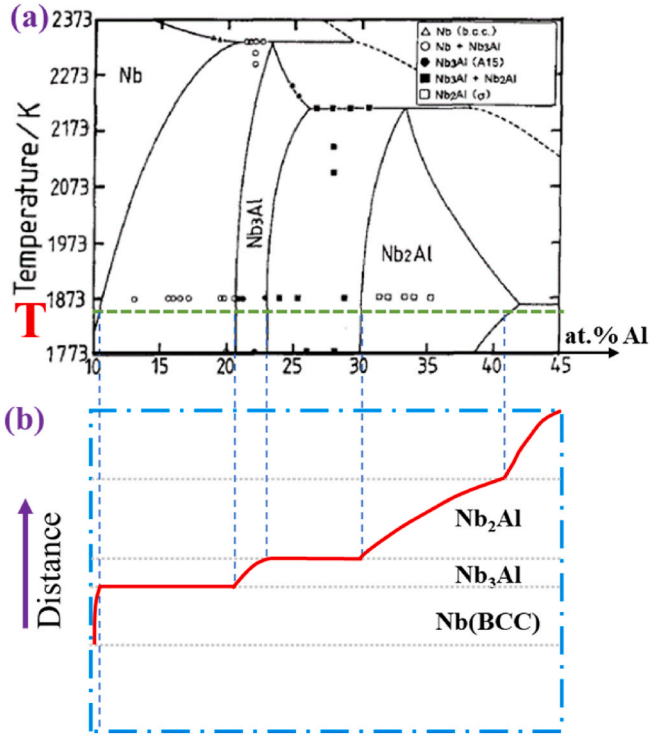

Fig. 2. (a) phase diagram of the binary system Nb-Al [40], (b) the concentration-penetration curve of component Al at temperature T.

atoms in TiAl melt need to pass through three intermetallic layers, and a concentration profile is established for Al element, as shown in Fig. 2(b). The reason is that, from the basic thermodynamic point of views, the creation of straight interface with fixed concentration gap in binary multiphases diffusion couples follows because of the phase rule govern it follows the only single-phase region can be formed in such a couple instead of two-phase regions. In contrast, in a ternary system, two-phase regions are allowed. It is assumed that the width of the Nb(BCC) (the melting point more than 2060 °C) phase layer and Nb_2Al phase layer are enough and the Nb(BCC)/Nb_2Al phase interface is flat, the interdiffusion of Nb and Al elements occur unidirectionally along the direction perpendicular to the interface (the diffusional direction). When the corrosion happens at temperature T for an appropriate time, the Nb_3Al phase will come into being at the interface due to the reactive diffusion between the Nb(BCC) and Nb_2Al phase. The concentration profile of Al element across the Nb_3Al phase along the diffusional direction is depicted in Fig. 3. The related the diffusion phenomenon correlates with the phase diagrams. The imperative standard is that the local equilibrium exists at the interfaces, but cannot be considered generally. For a short corrosion time, concentrations which departure from equilibrium diagram could certainly occur result from different surface energy, but for long corrosion time, deviations from equilibrium conditions at phase interface are reported [20,39]. The relation between the diffusion phenomenon and the phase diagram is then less obvious, even though in

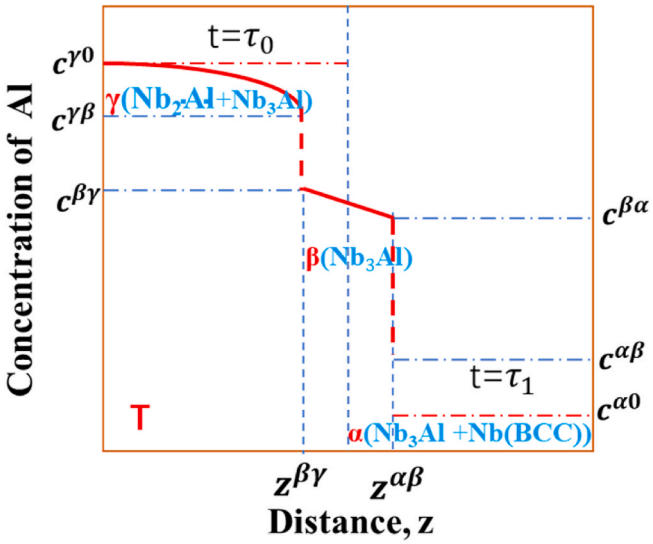

Fig. 3. Concentration outline of element Al across the β phase along the diffusional direction with initial compositions of $c^{\gamma 0}$ and $c^{\alpha 0}$ in γ and α, respectively. Dashed lines and solid curves show the concentration profiles before and after corrosion, respectively, and $z^{\beta\gamma}$ and $z^{\alpha\beta}$ indicate the positions of the γ/β and βα interfaces, respectively, after corrosion. α: Nb_3Al + Nb(BCC), β: Nb_3Al, γ: Nb_3Al + Nb_2Al.

some cases metastable extensions of equilibrium lines might be helpful in understanding these deviations. In some cases, however, these deviations are only apparent. If the local equilibrium is achieved at each migrating interface during T, the compositions of neighboring phases at the interface are identical to the corresponding phase boundaries in the phase as shown in Figs. 3 and 4. Such a reaction will actually begin on the assumption that the interface diffusion across the migrating interface is much faster than the volume diffusion in each phase.

The exact profile in the various phases cannot be predicted unless the interdiffusion coefficients are known as a function of composition. However, the concentration values of Nb_3Al + Nb(BCC)/Nb_3Al, Nb_3Al/Nb_2Al + Nb_3Al and Nb_2Al + Nb_3Al/Nb_2Al interfaces can be taken from the phase diagram if equilibrium conditions prevail at these interfaces.

The migration rate $dz^{\beta\gamma}/dt$ is related to the flux balance at the Nb_2Al + Nb_3Al/Nb_3Al interface.

$$\left(c^{\gamma\beta} - c^{\beta\gamma}\right)\frac{dz^{\beta\gamma}}{dt} = J^{\gamma\beta} - J^{\beta\gamma} \tag{1}$$

Similarly, the following equation can be obtained for interface Nb_3Al + Nb(BCC)/Nb_3Al.

$$\left(c^{\beta\alpha} - c^{\alpha\beta}\right)\frac{dz^{\alpha\beta}}{dt} = J^{\beta\alpha} - J^{\alpha\beta} \tag{2}$$

According to Fick's first law, the diffusional flux J^{ω} is proportional to the concentration gradient $\partial c^{\omega}/\partial x$ as follows.

$$J^{\omega} = -D^{\omega}\left(\frac{\partial c^{\omega}}{\partial x}\right) \tag{3}$$

In Eq. (3), D^{ω} is the diffusion coefficient for the volume diffusion in the ω phase, where ω stands for Nb_3Al + Nb(BCC), Nb_3Al and Nb_3Al + Nb_2Al phases. When the diffusion coefficient D^{ω} is independent of the composition of the ω phase, Fick's second law should be described by Eq. (4):

$$\frac{\partial c^{\omega}}{\partial x} = D^{\omega}\left(\frac{\partial^2 c^{\omega}}{\partial x^2}\right) \tag{4}$$

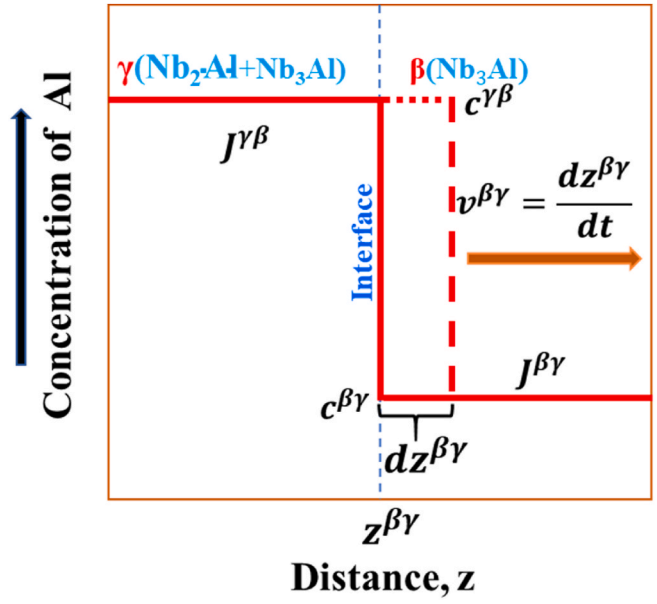

Fig. 4. Magnified concentration profile of element Al across the γ/β interface along the diffusional direction is regarded as almost flat because of the local equilibrium. The differential coefficient $dz^{\beta\gamma}/dt$ corresponds to the migration rate $v^{\beta\gamma}$ of the γ/β interface. $J^{\gamma\beta}$ and $J^{\beta\gamma}$ are the diffusional fluxes of element Al due to the volume interdiffusion in the γ and β phases, respectively, at the interface. α: Nb_3Al + Nb(BCC), β:Nb_3Al, γ: Nb_3Al + Nb_2Al.

Eq. (4) obviously demonstrates that the concentration c^{ω} is a function of the diffusion distance *x* and the corrosion time t.

The solution of Eq. (4) is

$$c^{\omega} = E + F\cdot\mathrm{erf}\left(x \Big/ \sqrt{4D^{\omega}t}\right) \tag{5}$$

In Eq. (5), E, F are constant decided by boundary conditions, where $\omega = \alpha, \beta$ *or* γ for the Nb_3Al + Nb(BCC), Nb_3Al, Nb_3Al + Nb_2Al phases, respectively.

For the Nb_3Al + Nb(BCC)/Nb_3Al + Nb_2Al diffusion couple, the initial conditions are expressed as

$$c^{Nb_3Al+Nb(BCC)}(x,\quad t=\tau_0) = c^{\alpha 0} \tag{6a}$$

$$c^{Nb_3Al+Nb_2Al}(x,\quad t=\tau_0) = c^{\gamma 0} \tag{6b}$$

On the other hand, the boundary conditions for the growth of the Nb_3Al phase are described by the equations

$$c^{Nb_3Al+Nb(BCC)}\left(x=z^{\alpha\beta},\quad t=\tau_1\right) = c^{\alpha\beta} \tag{7a}$$

$$c^{Nb_3Al}\left(x=z^{\alpha\beta},\quad t=\tau_1\right) = c^{\beta\alpha} \tag{7b}$$

$$c^{Nb_3Al}\left(x=z^{\beta\gamma},\quad t=\tau_1\right) = c^{\beta\gamma} \tag{7c}$$

$$c^{Nb_3Al+Nb_2Al}\left(x=z^{\beta\gamma},\quad t=\tau_1\right) = c^{\gamma\beta} \tag{7d}$$

Under such initial and boundary conditions, Eq. (5) can be solved analytically. An analytical solution will be explained in detail below.

The most intriguing aspect of this study is that the position $z^{\beta\gamma}$ of the moving interface are expressed as functions of time. In Fig. 5(a), the scale of the abscissa is extremely magnified to assess the migration distance $dz^{\beta\gamma}$ of the interface during the infinitesimally short time dt.

During the growth of the layer β simultaneous advancement of the β/γ interface boundaries will occur because of the accumulation of Al atom at the interface driving by the different concentration of Al in γ, β phases, which will generate a concentration gradient dc/dz near the interface, and the interface velocity will be controlled by this concentration gradient. Hence, the rule of mass conservation at the β/γ interface.

If it is assumed that the interface area is unit area and the interface is pushed forward $dz^{\beta\gamma}$ distance in dt time, so that the $dz^{\beta\gamma}$ volume of Al diffusion into the β phase, and the diffusional flux of Al into the β phase is $(C^{\gamma\beta} - C^{\beta\alpha})dz^{\beta\gamma}$. According to Fick's first law, the amount of Al passes through the β/γ interface per unit area is $D^{\gamma}\frac{dc}{dz}dt$. At the β/γ interface, the flux balance.

$$\left(C^{\gamma\beta} - C^{\beta\alpha}\right)\ dz^{\beta\gamma} = D^{\gamma}\frac{dc}{dz}dt \tag{8}$$

The interface migration speed is:

$$v^{\beta\gamma} = \frac{dz^{\beta\gamma}}{dt} = \frac{D^{\gamma}\left(\frac{dc}{dz}\right)}{(C_S - C_I)} \tag{9}$$

For quantitative calculation, the interface concentration profile can be simplified as a linear one, as shown in Fig. 5(b). Which leads to

$$\frac{dc}{dz^{\beta\gamma}} = \frac{\left(C^{\beta\alpha} - C^{\alpha\beta}\right)}{h} \tag{10}$$

According to the solute mass conservation, it is required that the two shaded area to be equal.

$$\left(C^{\gamma\beta} - C^{\beta\alpha}\right)\ z^{\beta\gamma} = \frac{1}{2}\left(C^{\beta\alpha} - C^{\alpha\beta}\right)\cdot h \tag{11}$$

And

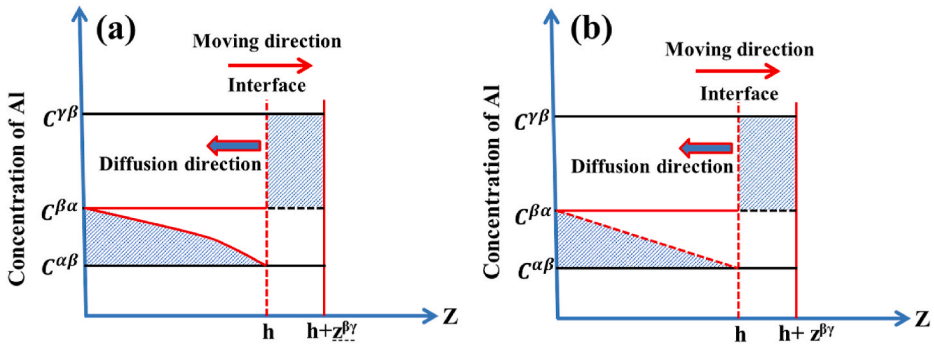

Fig. 5. Schematic representation of Al distribution caused by interface moving with thickness of z: (a) the real one, (b) the simple one. α: Nb_3Al + Nb(BCC), β:Nb_3Al, γ: Nb_3Al + Nb_2Al.

$$\frac{dc}{dz^{\beta\gamma}} = \frac{\left(C^{\beta\alpha} - C^{\alpha\beta}\right)^2}{2\left(C^{\gamma\beta} - C^{\beta\alpha}\right)\ z^{\beta\gamma}} \tag{12}$$

Integrate both sides simultaneously to obtain:

$$z^{\beta\gamma} = \frac{\left(C^{\beta\alpha} - C^{\alpha\beta}\right)\sqrt{D^{\gamma}t}}{\sqrt{\left(C^{\gamma\beta} - C^{\beta\alpha}\right)\left(C^{\beta\alpha} - C^{\alpha\beta}\right)}} \tag{13}$$

If the moving distance of the interface is very small, then $(C^{\gamma\beta} - C^{\beta\alpha}) \approx (C^{\beta\alpha} - C^{\alpha\beta})$.

$$z^{\beta\gamma} = \frac{\left(C^{\beta\alpha} - C^{\alpha\beta}\right)\sqrt{D^{\gamma}t}}{\left(C^{\gamma\beta} - C^{\beta\alpha}\right)} \tag{14}$$

and

$$v^{\beta\gamma} = \frac{dz}{dt} = \frac{\left(C^{\beta\alpha} - C^{\alpha\beta}\right)}{2\left(C^{\gamma\beta} - C^{\beta\alpha}\right)}\sqrt{\frac{D^{\gamma}}{t}} \tag{15}$$

Here, $\varepsilon^{\beta\gamma}$ is defined as the dimensionless proportionality coefficients

$$\varepsilon^{\beta\gamma} = \frac{\left(C^{\beta\alpha} - C^{\alpha\beta}\right)}{\left(C^{\gamma\beta} - C^{\beta\alpha}\right)} \tag{16}$$

The positions $z^{\beta\gamma}$ and $z^{\alpha\beta}$ of the migrating Nb_3Al/Nb_3Al + Nb_2Al and Nb_3Al + Nb(BCC)/Nb_3Al interfaces are expressed as functions of the annealing time t by the equations

$$z^{\beta\gamma} = \varepsilon^{\beta\gamma}\sqrt{4D^{\beta}t} = \varepsilon^{\gamma\beta}\sqrt{D^{\gamma}t} \tag{17}$$

Similarly, for α/β interface,

$$z^{\alpha\beta} = \varepsilon^{\alpha\beta}\sqrt{4D^{\alpha}t} = \varepsilon^{\beta\alpha}\sqrt{D^{\beta}t} \tag{18}$$

Here, D^{α}, D^{β}, D^{γ} are the diffusion coefficient for the volume diffusion in the Nb_3Al + Nb(BCC), Nb_3Al, Nb_3Al + Nb_2Al phase, respectively. $\varepsilon^{\alpha\beta}$, $\varepsilon^{\beta\alpha}$, $\varepsilon^{\beta\gamma}$, $\varepsilon^{\gamma\beta}$ are the dimensionless proportionality coefficients.

From Eq. (7), the following relationships are obtained

$$\varepsilon^{\beta\gamma} = \varepsilon^{\gamma\beta}\sqrt{D^{\gamma}/D^{\beta}} \tag{19a}$$

$$\varepsilon^{\alpha\beta} = \varepsilon^{\beta\alpha}\sqrt{D^{\beta}/D^{\alpha}} \tag{19b}$$

As can be seen in Fig. 2, the thickness l of the β phase is readily obtained as the difference between $z^{\alpha\beta}$ and $z^{\beta\gamma}$. According to Eq. (7), l is described as a function of t by the equation

$$l^2 = \left(z^{\alpha\beta} - z^{\beta\gamma}\right)^2 = 4D^{\beta}\left(\varepsilon^{\alpha\beta} - \varepsilon^{\beta\gamma}\right)^2 t = Kt \tag{20}$$

$$l = \sqrt{Kt} \tag{21}$$

Here, the kinetics coefficient K in Eq. (11) is defined as

$$K = 4D^{\beta}\left(\varepsilon^{\alpha\beta} - \varepsilon^{\beta\gamma}\right)^2 \tag{22}$$

Theoretically, the β phase layer growth is a function of time suggests that this phase emerges as a result of interdiffusion process. And more than one intermetallic compound layer formed due to the migration of their interfaces are diffusion-controlling process. And this calculation result is coincident and consistent with an empirical expression summarized by Son and Morral [26] and Kajihara's calculational result in a hypothetical binary system [25]. Therefore, the reactive diffusion taking place on the surface of Nb container obeys parabolic kinetics and can be expressed by the relationship in Eq. (20) and Eq. (21). It is concluded that the growth of intermetallic compounds layer is controlled by the diffusion of Al element in present paper.

4. Results and discuss

4.1. Experimental verification of growth kinetics of intermetallic layers

Fig. 6 shows the microstructure of the interface between Nb container and TiAl melt at 1600 °C for different corrosion time and the corresponding line scanning analysis of the chemistry composition of Al, Nb and Ti elements. As mentioned before, it is note that the boundary contour profile of the intermetallic compound is not obvious in the interfacial region, as shown in Fig. 6(a, c, e, g, i). In contrast, the corresponding line scanning analysis reveals that there are new phases forming based on the concentration profiles, especially for Al and Nb elements, are discontinuous with some distinct steps in it, as revealed in Fig. 6(b, d, f, h, j), which are closely related to the phase diagram of Nb–Al system, as presented in Fig. 2(a and b) and Fig. 4. Accordingly, the thickness of intermetallic layers can be measured.

For the purpose of quantitative evaluation of the intermetallic compounds layer growth kinetics, the thickness of different intermetallic compounds layer needs to be knew. Even though some discrepancies in the compositions of the Nb_3Al phase boundaries still remain, a consensus is made that the Nb_3Al phase with compositions from 21 to 23 mol% Al is a single phase at 1600 °C [41–45], which is coincident and consistent with the data shown in phase diagram (Fig. 2), as depicted in Fig. 8. It is implied that the rationality of the data from the phase diagram at this temperature. What's more, it is interesting to note that the thickness of intermetallic compound layers region obtained by the components origin from the phase diagram fall exactly between the two small steps. This is correlate well with Van Loo's opinions [27]. Accordingly, the thickness of different intermetallic compound layers can be obtained based on Fig. 6(b, d, f, h, j), and the relevant data as revealed in Table 1. Otherwise, based on our previous study [38], O2, α2, γ phases can be founded in the boundary of TiAl alloy side.

In order to figure out the growth kinetics of the intermetallic compound layers, the square root of time dependence of the corresponding intermetallic compounds layers measurement thickness based on phase

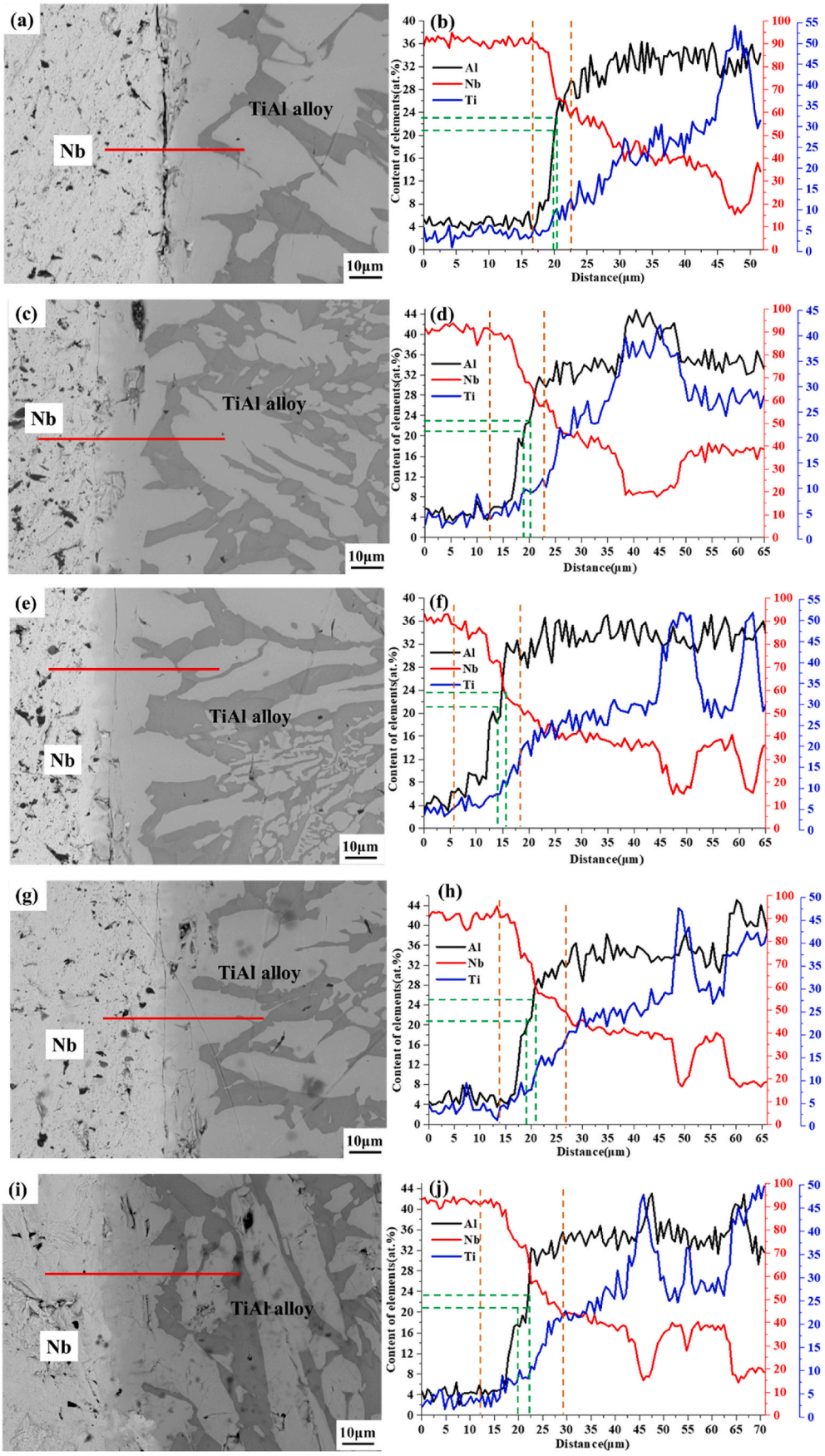

Fig. 6. The microstructure of the interfacial regions at 1600 °C and the corresponding line scanning analysis of Al, Nb and Ti elements along the line with different corrosion time: (a)1.39h, (b)1.55h, (c)1.74h, (d)1.95h, (e)2.15h.

Table 1
The thickness of different intermetallic compound layers for different corrosion time at 1600 °C. (α: Nb_3Al + Nb(BCC), β:Nb_3Al, γ: Nb_3Al + Nb_2Al.).

	(a)	(b)	(c)	(d)	(e)
Corrosion time (h)	1.39	1.55	1.74	1.95	2.15
Thickness of Nb (BCC)+Nb_3Al + Nb_2Al (μm)	4.783 ± 0.3	7.096 ± 0.1	8.882 ± 0.5	11.614 ± 0.4	14.335 ± 0.5
Thickness of α(Nb (BCC)+Nb_3Al) (μm)	2.525 ± 0.2	3.373 ± 0.1	4.154 ± 0.3	5.385 ± 0.2	6.596 ± 0.3
Thickness of β(Nb_3Al) (μm)	0.652 ± 0.15	1.293 ± 0.1	1.727 ± 0.1	2.203 ± 0.1	2.736 ± 0.1
Thickness of γ(Nb_3Al + Nb_2Al) (μm)	4.216 ± 0.3	5.49 ± 0.2	6.527 ± 0.1	7.981 ± 0.2	8.702 ± 0.3

diagram and the relevant linear fitting are established, as shown in Fig. 7. It can be seen that the growth thickness of intermetallic compounds layers increases linearly with the square root of corrosion time, the kinetic constants and the correlation coefficients are shown in Table 2, indicating that the growth of intermetallic compounds layers are controlled by the diffusion of Al element. It has been found that good agreement with the theoretical derivation relation.

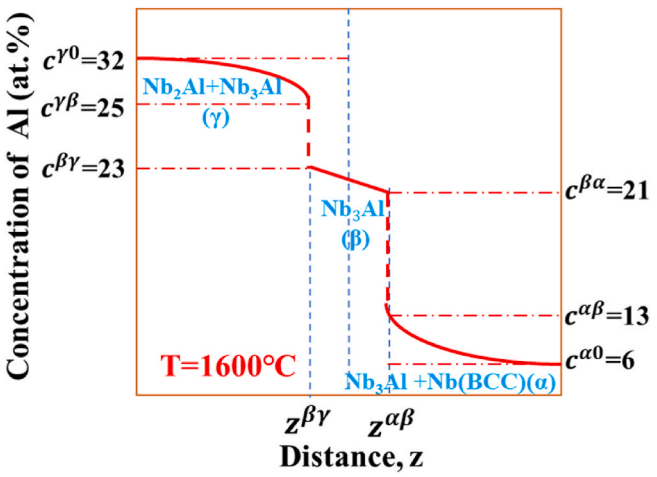

Fig. 8. Concentration profile of element Al across the Nb_3Al phase along the diffusional direction in the diffusion couple according to phase diagram at 1600 °C.

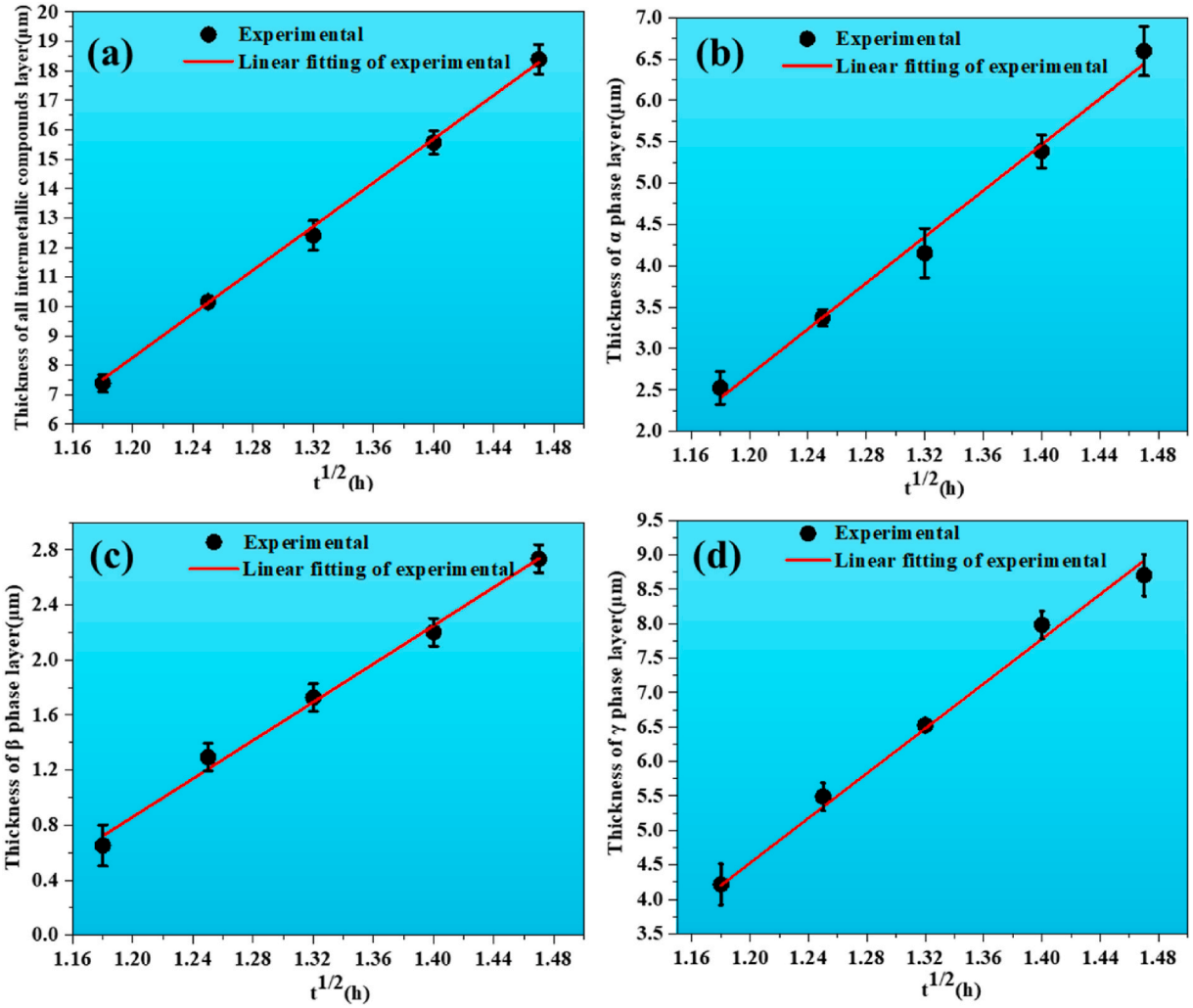

Fig. 7. The square root of corrosion time dependence of the corresponding intermetallic compounds layers measurement thickness: (a)the total, (b) α phase, (c) β phase, (d) γ phase. α: Nb_3Al + Nb(BCC), β:Nb_3Al, γ: Nb_3Al + Nb_2Al.

Table 2
The kinetic constants and correlation coefficients obtained by linear fitting.

(α: Nb_3Al + Nb(BCC), β:Nb_3Al, γ: Nb_3Al + Nb_2Al.)		
Intermetallic compound layers	the kinetics coefficient K ($(\mu m)^2/h$)	R-Square
the total	1375.67	0.997
α(Nb_3Al + Nb(BCC))	193.77	0.989
β(Nb_3Al)	48.3	0.997
γ(Nb_3Al + Nb_2Al)	264.06	0.986

4.2. Discussing the effects on growth kinetics of the intermetallic compound layers

In the previous section a diffusion model is developed, in terms of error function solutions for Fick's second law and the mass conservation law. In order to quantitatively estimate the growth kinetics of intermetallic compounds layers at a certain temperature. Both Al diffusion through the intermetallic compound phases and anomalous Al diffusion through the Nb phase are properly analyzed to account for in the calculations and experiments.

According to the phase diagram (Fig. 2(a)) at 1600 °C, the concentration profile of element Al across the associated intermetallic compounds phase and the boundary concentration along the diffusional direction like Fig. 8. Consequently, the determination of the dimensionless proportionality coefficient $\varepsilon^{\beta\gamma}$ is carried out using Eq. (16), similarly, the values of $\varepsilon^{\alpha\beta}$, $\varepsilon^{\gamma\alpha}$ can be obtained. But considering that the Al element concentration range is 21 to 23 at.% and closing to the calculation of the dimensionless proportionality coefficient, we define:

$$\varepsilon_1 = \frac{c^{\alpha\beta} - c^{\alpha 0}}{c^{\beta\alpha} - c^{\alpha\beta}} \tag{23a}$$

$$\varepsilon_2 = \frac{c^{\beta\alpha} - c^{\alpha\beta}}{c^{\beta\gamma} - c^{\alpha\beta}} \tag{23b}$$

$$\varepsilon_3 = \frac{c^{\beta\gamma} - c^{\beta\alpha}}{c^{\gamma\beta} - c^{\beta\gamma}} \tag{23c}$$

$$\varepsilon_4 = \frac{c^{\gamma\beta} - c^{\beta\gamma}}{c^{\gamma 0} - c^{\gamma\beta}} \tag{23d}$$

Combined with Fig. 8, the values of ε_1, ε_2, ε_3, ε_4 can be obtained, as shown in Table 3. According to Eq. (22), the kinetics coefficient K is characterized by the dimensionless proportionality coefficient defined by Eq. (23(a-d)), the diffusion coefficient D^{ω} can be calculated connection with Tables 2 and 3, the calculation results are shown in Fig. 9. It can be seen that the diffusion coefficient of Al element in the β phase is much smaller than those of in the α and γ phases, that of in γ phase is the largest. This is the reason why the β phase layer cannot be seen in the boundary layer, in contrast, γ phase layer can easily be detected. It is demonstrated that a long time needs for Al atoms get though β phase layer and α phases layer, therefore, β and α phases layers can be regarded as the corrosion resistance layers. Which is in agreement well with the experiment results. On the other hand, as shown in Fig. 4, the concentration profile of Al element is depicted as a straight line. In such a case, the following approximation may be sometimes applied for estimating the diffusion flux of Al element in β phase based on Eq. (3).

$$J^{\beta} = -D^{\beta}\frac{(c^{\beta\gamma} - c^{\beta\alpha})}{l} \tag{24}$$

Eq. (24) demonstrates that the diffusion flux of Al element in β phase J^{β} is proportional to the product of D^{β} and $c^{\beta\gamma} - c^{\beta\alpha}$. And which is the theoretical basis of approximation Eq. 22(a-d). As a consequence, the effect of $c^{\beta\gamma} - c^{\beta\alpha}$ on K becomes comparable to that of D^{β}. According to Eq. (19) and Eq. (22), $D^{\beta}/D^{\alpha} = 0.27$, $D^{\beta}/D^{\gamma} = 1.02 \times 10^{-2}$, thus, K becomes very insensitive to $c^{\beta\gamma} - c^{\beta\alpha}$, which implies that the β phase thickness is predominantly determined by D^{β}. What's more, taking an existing concentration gradient into consideration, which implies that the β phase thickness is predominantly affected initial compositions of the α and γ phases based on Eq. (20). Therefore, it is concluded that the solubility range of α and γ phases in β phase has a significant effect on the growth rate of β phase at this temperature. However, it is indicated that both Nb(BCC) and Nb_2Al phases do not dissolve easily in Nb_3Al phase at 1600 °C [40]. Hence, the effect of solubility is not as obvious as that of Al diffusion. It is concluded that a long corrosion time would be taken to reach to an observable thickness for the intermetallic compound layer with a small diffusion coefficient and a narrow solubility range. From the corrosion resistance perspective, the formation of β and α phases layers can improve the corrosion resistance ability effectively during a certain corrosion time. This is in agreement with the experimental results shown in Fig. 6.

Table 3
The calculation values of ε_1, ε_2, ε_3, ε_4.

ε_1	ε_2	ε_3	ε_4
0.875	4	1	0.286

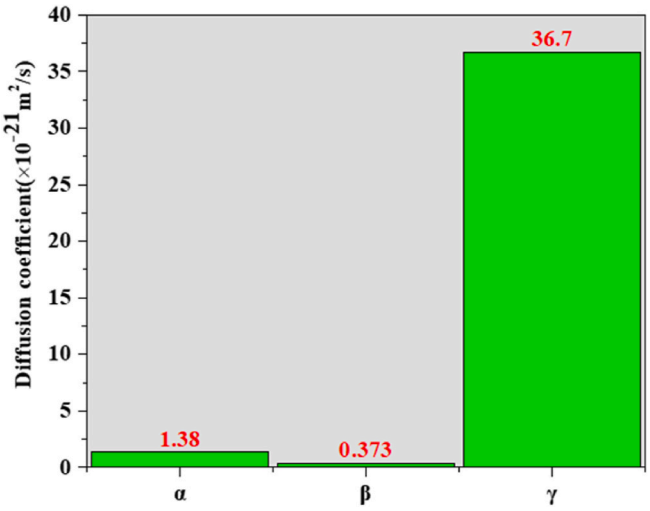

Fig. 9. The diffusion coefficients of Al element in α, β and γ phases. α: Nb_3Al + Nb(BCC), β:Nb_3Al, γ: Nb_3Al + Nb_2Al.

With increasing thickness of the diffusion zones, the influence of interfacial interaction barriers increases and the simultaneous existence of diffusion controlled growth of all equilibrium phases is expected [46]. Therefore, it is necessary to establish the relationship the composition c^{ω} is expressed as a function of the distance Z and the corrosion time t.

Inserting Eq. (6) and Eq. (7) into Eq. (5), the following relationship are obtained.

$$c^{\beta\alpha} - c^{\alpha\beta} = \frac{c^{\alpha 0} - c^{\alpha\beta}}{\varepsilon^{\alpha\beta}\sqrt{\pi}[1 - \mathrm{erf}(\varepsilon^{\alpha\beta})]}\exp\left[-\left(\varepsilon^{\alpha\beta}\right)^2\right] + \frac{c^{\beta\gamma} - c^{\beta\alpha}}{\varepsilon^{\beta\alpha}\sqrt{\pi}[\mathrm{erf}(\varepsilon^{\beta\alpha}) - \mathrm{erf}(\varepsilon^{\beta\gamma})]}\exp\left[-\left(\varepsilon^{\beta\alpha}\right)^2\right] \tag{25}$$

and

$$c^{\gamma\beta} - c^{\beta\gamma} = \frac{c^{\beta\alpha} - c^{\beta\gamma}}{\varepsilon^{\beta\gamma}\sqrt{\pi}[\mathrm{erf}(\varepsilon^{\beta\alpha}) - \mathrm{erf}(\varepsilon^{\beta\gamma})]}\exp\left[-\left(\varepsilon^{\beta\gamma}\right)^2\right] + \frac{c^{\gamma 0} - c^{\gamma\beta}}{\varepsilon^{\gamma\beta}\sqrt{\pi}[1 + \mathrm{erf}(\varepsilon^{\beta\gamma})]}\exp\left[-\left(\varepsilon^{\gamma\beta}\right)^2\right] \tag{26}$$

All the independent variables are obtained, the composition c^{ω} is expressed as a function of the distance Z and the corrosion time t by the following equations for the Nb_3Al + Nb(BCC), Nb_3Al and Nb_3Al + Nb_2Al phases can be gotten.

$$c^{\alpha} = c^{\alpha 0} + \frac{c^{\alpha\beta} - c^{\alpha 0}}{1 - \mathrm{erf}(\varepsilon^{\alpha\beta})}\left[1 - \mathrm{erf}\left(\frac{Z}{\sqrt{4D^{\alpha}t}}\right)\right], (Z > z^{\alpha\beta}) \quad (27)$$

$$c^{\beta} = \frac{c^{\beta\gamma}}{\mathrm{erf}(\varepsilon^{\beta\alpha}) - \mathrm{erf}(\varepsilon^{\beta\gamma})}\left[\mathrm{erf}(\varepsilon^{\beta\alpha}) - \mathrm{erf}\left(\frac{Z}{\sqrt{4D^{\beta}t}}\right)\right] - \frac{c^{\beta\alpha}}{\mathrm{erf}(\varepsilon^{\beta\alpha}) - \mathrm{erf}(\varepsilon^{\beta\gamma})}\left[\mathrm{erf}(\varepsilon^{\beta\gamma}) - \mathrm{erf}\left(\frac{Z}{\sqrt{4D^{\beta}t}}\right)\right], (z^{\beta\gamma} < Z < z^{\alpha\beta}) \quad (28)$$

$$c^{\gamma} = c^{\gamma 0} + \frac{c^{\gamma\beta} - c^{\gamma 0}}{1 + \mathrm{erf}(\varepsilon^{\gamma\beta})}\left[1 + \mathrm{erf}\left(\frac{Z}{\sqrt{4D^{\gamma}t}}\right)\right], (Z < z^{\beta\gamma}) \quad (29)$$

Combining Fig. 9 and Table 3 Eqs.27–29 can be materialized Eqs. 30–32.

$$c^{\alpha} = 0.06 + 0.45\left[1 - \mathrm{erf}\left(\frac{Z}{2.35 \times 10^{-6}\sqrt{t}}\right)\right] \quad (30)$$

$$c^{\beta} = 0.205 + 0.03\mathrm{erf}\left(\frac{Z}{3.05 \times 10^{-7}\sqrt{t}}\right) \quad (31)$$

$$c^{\gamma} = 0.258 + 0.062\mathrm{erf}\left(\frac{Z}{1.01 \times 10^{-5}\sqrt{t}}\right) \quad (32)$$

In Eqs. 30–32, the relationship between the migration distance of the phase boundary layer and the corrosion time is established because of the concentration of the related parameters can be obtained based on phase diagram at 1600 °C.

4.3. The diffusion depth evaluation of Al in Niobium

In our research, we do not only understand the growth law of intermetallic compounds layers, but the kinetics of the interaction between the TiAl melt and Nb container, which will be beneficial for understanding or predicting the diffusion process further. According to Fig. 7(a), the total mean thickness of the reaction layer is diffusion-controlling, therefore, the interdiffusion of elements at a certain temperature can be described by Eq. (20):

$$l^2 = K_1 t$$

where l is the total mean thickness of Al element diffusion, K is the kinetics constant, t is the diffusion time.

In order to calculate the mean depth of Al diffuses into Nb, it is necessary to calculate the kinetics constant and establish the relationship between the kinetics constant and the temperature T. Apparent activation energy Q (kJ/mol) for diffusion-controlled can be obtained from Arrhenius relation:

$$K_1 = K_0 \exp\left(-\frac{Q}{RT}\right) \quad (33)$$

Eq. (32) is linearized by taking the natural logarithm,

$$\ln K_1 = \ln K_0 - \frac{Q}{RT} \quad (34)$$

The values of Q = 51.88 kJ/mol and $K_0 = 4.5 \times 10^{-5}$ m^2/s can be obtained from the result revealed in Fig. 10. This activation energy only presents that the Al atoms in TiAl melt diffuse into pure Nb to form extensive b.c.c solid solution. The diffusion mechanism is that the Al atoms jump into the nearest-neighbor single Nb vacancies.

The activation energy Q and the kinetics constant K are substituted into Eq. (35) and Eq. (20), and the mean depth of Al diffuse into Nb can be characterized by the following equation:

$$l^2 = 4.5 \times 10^{-5} \exp\left(-\frac{51.88 \times 10^3}{RT}\right) t \quad (35)$$

When T = 1600 °C, Eq. (36) can be materialized

$$l^2 = 1.6 \times 10^{-6} t \quad (36)$$

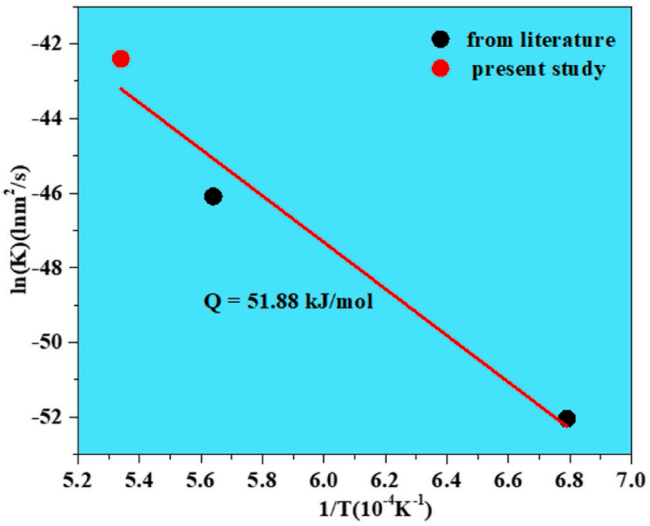

Fig. 10. Arrhenius plot of kinetics constants K for Al in niobium phase versus the temperature T from the present study and from the literature [33,47].

Only the diffusion of Al in Nb are considered in Eqs. (36) and (37), and the role of intermetallic compounds formed at interface is not taken into consideration, nor do the influence of the formed intermetallic compound layer on diffusion. In fact, through the previous study, intermetallic compound layers are formed during the interfacial interaction, which makes Al diffusion in Nb more complex. And according to the experimental results linear regression analysis shown in Fig. 11, we can get the experimental relationship between the diffusion distance and corrosion time:

$$l^2 = 1.67 \times 10^{-12} t \quad (37)$$

Fig. 11 reveals the connection between the average depth of Al diffusion into Nb from experimental. By comparison, it is note-worthy that the calculated value is three orders of magnitude higher than the experimental value under the same corrosion time. The reason is that, thermodynamically, the calculated activation energy is low, which reveals Al may diffuse far away into Nb, therefore, the predicted diffusion depth is greater than the actual result. In fact, there existing three intermetallic compound layers and the apparent activation energy of Al in Al_3Nb is about 127 kJ/mol [36], and that of in Nb_2Al is reported as

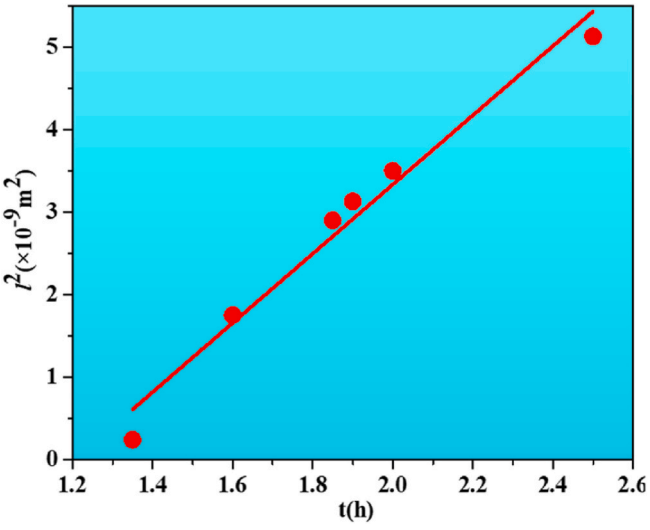

Fig. 11. The experimental mean depth of Al diffuses into Nb versus the corrosion time.

230 kJ/mol [48] and in Nb_3Al is 366 kJ/mol [49], which are more than 51.88 kJ/mol. Therefore, higher temperature or longer time is required to stimulate Al diffusion through intermetallic compound layers and corrode Nb container further. It is indicated that the intermetallic compounds formed indeed play a crucial role in hindering Al diffusion. What's more, β phase formed firstly to some degree when Al diffuse into Nb by thermodynamical calculation [50], however, the previous calculation reveals the diffusion coefficient of β is only 0.373×10^{-21} m^2s^{-1}, as shown in Fig. 9, which is far less than the diffusion coefficient of γ, it is concluded that the intermetallic compound β layer is a dominant factor for hindering Al diffusion, in other words, there are clear intrinsic barriers that limit Al significant further diffusion. Therefore, it is difficult to observe the phase morphology during the experiment, which is consistent with the previous experimental results. Therefore, the conclusion can be drawn that the growth kinetics of intermetallic compound layer have a positive effect on the resistance corrosion about them. At the same time, it is implied that compared with the thermodynamic factors the kinetic factors can be the dominant controlling factor, this could be in agreement with the analysis in section 4.2.

4.4. The corrosion average thickness of Nb vs corrosion time

Fig. 12 shows SEM images of cross-sectional microstructures of the Nb container/TiAl alloy interface for 1.5h corrosion. Intermetallic compounds layer can be easily found at the interface between TiAl alloy and Nb container, as shown in Fig. 12(a). The mappings of Ti, Al, Nb, O elements demonstrate that interdiffusion of Ti, Al elements and Nb occurred at the interface and an overt concentration gradient existed in the bulk of the intermetallic phases in Fig. 12(b, c, d, e), especially, Al [Fig. 12(d)] and Nb [Fig. 12(c)]. What's more, α layer, β layer, and γ layer can be observed clearly [Fig. 12(a)]. It is concluded that the formed intermetallic compound layers hinder the interdiffusion of Ti, Al and Nb. It is interesting to note that oxygen is mainly distributed near the crack based on Fig. 12 (f), demonstrating there is almost no oxygen in the intermetallic compound layer.

The effects on growth kinetics of intermetallic layers are discussed and the diffusion coefficient of β is far less than the diffusion coefficient of α and γ, which leads to the thickness of β layer be small, in contrast, the thickness of α and γ layers are relatively large, as shown in Fig. 12(a). To underline this point, TEM analysis is used to prove the relevant phase, as shown in Fig. 13. The distinct intermetallic compounds layers

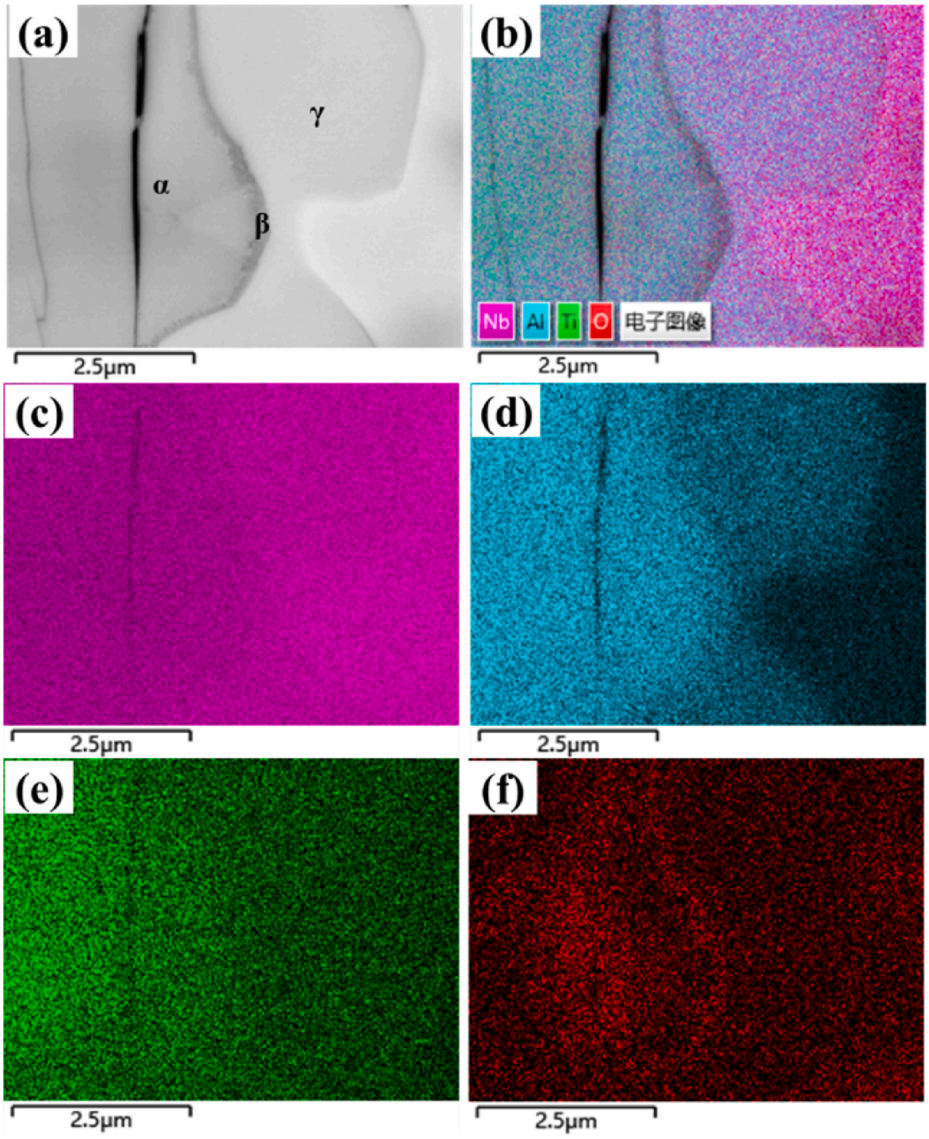

Fig. 12. SEM images of cross-sectional microstructures of the Nb container/TiAl alloy interface for 1.5h corrosion: (a) SEM-BSE image, (b) Nb, (c) Ti, (d) Al (e) Ti, (f) Al mapping in (a). α: Nb_3Al + Nb(BCC), β:Nb_3Al, γ: Nb_3Al + Nb_2Al.

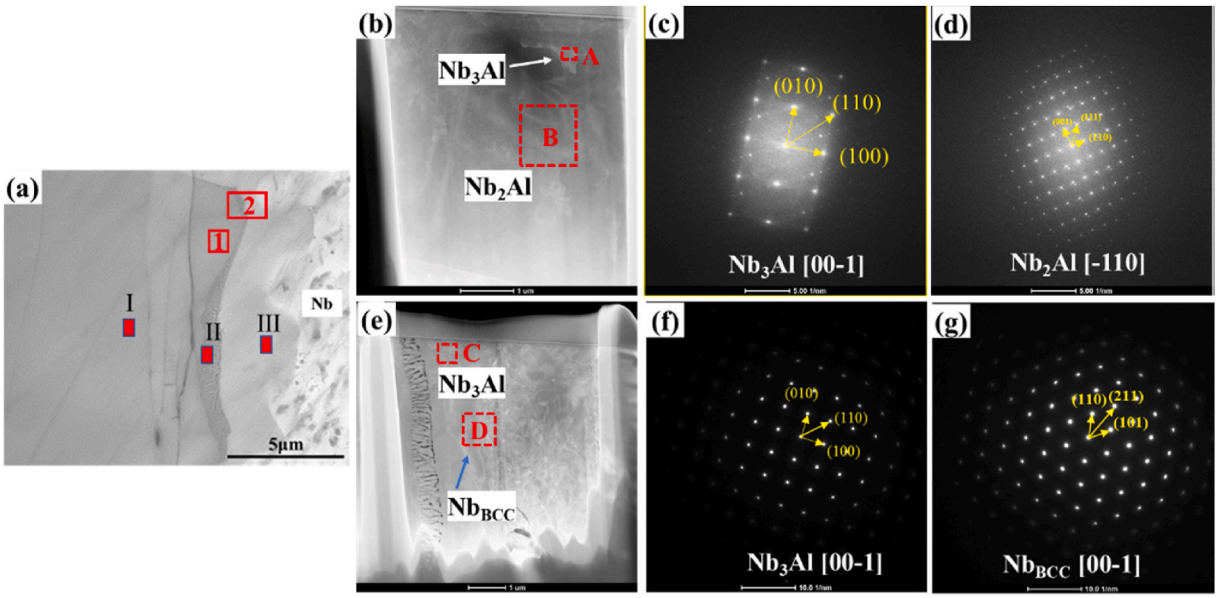

Fig. 13. (a) SEM-BSE micrograph of heat treatment of experimental sample for corrosion 1.5h. (b) Bright-field TEM micrograph of a flat specimen prepared from 1 zone in (a). This specimen was prepared with the focused-ion-beam (FIB) technology. (c) A corresponding selected-area electron diffraction (SAED) pattern collected from A colony (Nb_3Al) in (b). (d) A corresponding SAED pattern collected from B colony (Nb_2Al) in (b). (e) Bright-field TEM micrograph of a flat specimen prepared from 2 zone in (a). This specimen was prepared with the FIB technology too. (f) A corresponding SAED pattern collected from C colony (Nb_3Al) in (e). (g) A corresponding SAED pattern collected from D colony (Nb_{BCC}) in (e).

are presented, and the relevant components revealed in Table 4, which indeed confirms that the α, β and γ phases precipitation shown in Fig. 13 (a). It is interesting to note that the precipitated β phase is approximately 1.5 μm in thickness and that of γ is about 3.5 μm, these are coherent with Fig. 7(c) and Table 1. Fig. 13(b) and (e) are bright-field TEM micrograph of a flat specimen prepared from 1 to 2 zone in (a) respectively, indicating γ phase consists of Nb_2Al (B zone) andNb_3Al (A zone) phases [the SAED patterns shown in Fig. 13(c and d)] and α phase includes Nb_3Al (C zone) and Nb(BCC) (D zone) phases [the SAED patterns shown in Fig. 13 (f and g)]. It is implied that the rationality of this approach. On the other hand, due to the diffusion coefficient of Al in β is only 0.373×10^{-21} m^2s^{-1}, the precipitation of β phase requires a longer holding time in terms of kinetics, and this is why there is invisible β phase in section 4.1.

The change of corrosion thickness of the Nb container with the corrosion time is plotted in Fig. 14. From the slopes of the curves, we calculated the corrosion rate of Nb, dL/dt, of this temperature. The erosion rate of Nb is relatively rapid at the initial before 2.5h and then lower rapidly with time, the reason of that is the intermetallic layers formed at the surface of Nb container could facilitate the corrosion resistance ability, which is in agreement with experimental and theoretical results. During the corrosion experiment, the corrosion thickness of Nb increases to about 300 μm with the lower corrosion rate of Nb to about 25 μm/h for 5h corrosion. It has been indicated that the intermetallic compounds resistance-corrosion sheet has a positive effect on inhibition of further corrosion. it is concluded that the intermetallic compounds layer formed in the surface of Nb container has a positive role in corrosion resistance at high temperature. This is well in agreement with section 4.4.

Table 4
the point results and the relevant components in Fig. 13(a) by EDS.

No.	Element			
	Al (at.%)	Nb(at.%)	Ti (at.%)	Phases
I	34.19	55.73	10.07	γ(Nb_2Al + Nb_3Al)
II	29.86	62.7	7.43	β(Nb_3Al)
III	19.12	76.14	4.74	α(Nb_3Al + Nb(BCC))

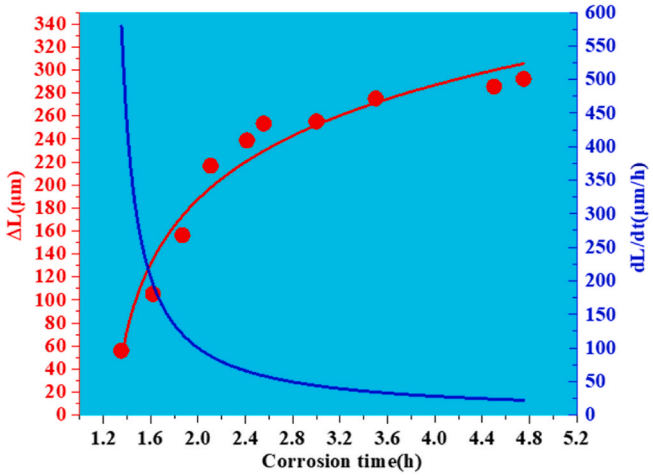

Fig. 14. The corrosion average thickness of Nb, ΔL, and corrosion rate of Nb, dL/dt, vs corrosion time at experimental temperature.

5. Conclusion

The growth kinetics of intermetallic compound is theoretically analyzed by reasonably simplifying Ti–Al–Nb ternary system to Nb–Al binary system. The kinetics relationship deduced may be valid based the present analysis results from the intermetallic compounds are thermodynamically stable. The effect of Al diffusion on the growth kinetics of intermetallic compounds at the interface between Nb container and TiAl melt was discussed and compared with relevant thermodynamic factors. The results of the study indeed confirm that the intermetallic compounds layer plays a dominant role in controlling the Al element diffusion and corrosion process. The conclusions are as follows:

1. The growth of the intermetallic compound layers are caused by the movement of the interface of the adjacent compound layers and

controlled by diffusion process. Theoretically, the growth kinetics follows the relationship $l = \sqrt{Kt}$.

2. Experimentally, the growth kinetics of Nb_3Al, Nb_3Al + Nb (BCC), and $Nb_3Al + Nb_2Al$ follow the parabolic relationship. At 1600 °C, the diffusion coefficients of Al in Nb_3Al, Nb_3Al + Nb(BCC), and $Nb_3Al + Nb_2Al$ are 0.373×10^{-21} m^2/s, 1.38×10^{-21} m^2/s, 36.7×10^{-21} m^2/s.
3. A diffusion model, which considers the successive diffusion of Al in Nb–Al intermetallic compounds as well as solid solution, is used to reasonable estimate Al diffusivity. The apparent diffusion activation energy of Al diffuse into Nb is 51.88 kJ/mol, and the relationship between the diffusion distance of Al and the corrosion time is $l^2 = 1.6 \times 10^{-6}t$.
4. The growth kinetics of intermetallic compounds layers are related to the corrosion resistance of the interface. The formation of the intermetallic compound layer makes the corrosion rate reduce an order of magnitude.

Declaration of competing interest

The authors declare that they have no known competing financial interests or personal relationships that could have appeared to influence the work reported in this paper.

Acknowledgements

This study was financially supported by Shanghai Sailing Program (19YF1420000).

References

[1] B. Bewlay, M. Weimer, T. Kelly, A. Suzuki, P. Subramanian, The science, technology, and implementation of TiAl alloys in commercial aircraft engines, MRS Proceedings 1516 (2013).
[2] H. Clemens, H. Kestler, Processing and applications of intermetallic γ-TiAl-based alloys, Adv. Eng. Mater. 2 (9) (2000) 551–570.
[3] H.L. Du, P.K. Datta, D. Hu, X. Wu, High temperature corrosion mechanisms of certain new TiAl-based intermetallic alloys in an aggressive $H_2/H_2O/H_2S$ environment at 850°C, Corrosion Sci. 49 (5) (2007) 2406–2420.
[4] G. Chen, Y. Peng, G. Zheng, Z. Qi, M. Wang, H. Yu, C. Dong, C.T. Liu, Polysynthetic twinned TiAl single crystals for high-temperature applications, Nat. Mater. 15 (8) (2016) 876–881.
[5] S. Yan, Z. Qi, Y. Chen, Y. Cao, J. Zhang, G. Zheng, F. Chen, T. Bian, G. Chen, Interlamellar boundaries govern cracking, Acta Mater. 215 (2021), 117091.
[6] Y. Chen, Y. Cao, Z. Qi, G. Chen, Increasing high-temperature fatigue resistance of polysynthetic twinned TiAl single crystal by plastic strain delocalization, J. Mater. Sci. Technol. 93 (2021) 53–59.
[7] J.B.F. Gomes, C.S. Ribeiro, Induction melting of γ-TiAl in CaO crucibles, Intermetallics 16 (11–12) (2018) 1292–1297.
[8] J. Lapin, A. Klimová, Vacuum induction melting and casting of TiAl-based matrix in-situ composites reinforced by carbide particles using graphite crucibles and moulds, Vacuum 169 (2019), 108930.
[9] N. Marié, K. Wolski, M. Biscondi, Grain boundary penetration of nickel by liquid bismuth as a film of nanometric thickness, Scripta Mater. 43 (10) (2000) 943–949.
[10] A.M. Gusak, K.N. Tu, C. Chen, Extremely rapid grain growth in scallop-type Cu6Sn5 during solid-liquid interdiffusion reactions in micro-bump solder joints, Scripta Mater. 179 (2020) 45–48.
[11] L. Zhu, J. Li, B. Tang, Y. Liu, M. Zhang, L. Li, H. Kou, Microstructure evolution and mechanical properties of diffusion bonding high Nb containing TiAl alloy to Ti2AlNb alloy, Vacuum 164 (2019) 140–148.
[12] R. Ma, Z. Liu, W. Wang, G. Xu, W. Wang, Laser deposition melting of TC4/TiAl functionally graded material, Vacuum 177 (2020), 109349.
[13] Q.B. Wang, Z.P. Hou, S.Z. Zhang, H. Feng, C.J. Zhang, J.C. Han, W.G. Zhang, R. T. Zhao, Pore structure and compression behavior of porous TiAl alloys by freeze casting, Vacuum 175 (2020), 109254.
[14] Z.J. Hu, R.F. Guo, S.M. Chen, Q. Jin, P. Shen, Synthesis of damage-tolerant Cu-matrix composites with nacre-inspired laminate-reticular hierarchical architecture via tuning compositional wettability, Scripta Mater. 186 (2020) 312–316.
[15] W. Deqing, S. Ziyuan, Z. Longjiang, A liquid aluminum corrosion resistance surface on steel substrate, Appl. Surf. Sci. 214 (1) (2003) 304–311.
[16] Y. Wang, J. Xing, H. Fu, Y. Liu, K. Zheng, S. Ma, Y. Jian, Interfacial morphology and corrosion-wear behavior of cast Fe-3.5wt.% B steel in liquid zinc, Corrosion Sci. 131 (2018) 290–299.
[17] G. Xu, K. Wang, X. Dong, H. Jiang, Q. Wang, B. Ye, W. Ding, Multiscale corrosion-resistance mechanisms of novel ferrous alloys in dynamic aluminum melts, Corrosion Sci. 163 (2020), 108276.
[18] M. Schaefer, R.A. Fournelle, J. Liang, Theory for intermetallic phase growth between cu and liquid Sn-Pb solder based on grain boundary diffusion control, J. Electron. Mater. 27 (11) (1998) 1167–1176.
[19] Z. Chen, Y. Zhao, Z. Zhang, Theoretical and experimental study of precipitation and coarsening kinetics of θ′ phase in Al-Cu alloy, Vacuum 189 (2021), 110263.
[20] G.V. Kidson, Some aspects of the growth of diffusion layers in binary systems, J. Nucl. Mater. 3 (1) (1961) 21–29.
[21] W.E. Sweeney, A.P. Batt, Electron probe and X-ray diffraction measurements of intermediate phases in Zr diffused with Cr, Fe, Ni, Cu and Mo, J. Nucl. Mater. 13 (1) (1964) 87–91.
[22] J. Shen, Y.C. Chan, S.Y. Liu, Growth mechanism of Ni_3Sn_4 in a Sn/Ni liquid/solid interfacial reaction, Acta Mater. 57 (17) (2009) 5196–5206.
[23] N. Matan, H.M.A. Winand, P. Carter, M. Karunaratne, P.D. Bogdanoff, R.C. Reed, A coupled thermodynamic/kinetic model for diffusional processes in superalloys, Acta Mater. 46 (13) (1998) 4587–4600.
[24] J.S. Park, K. Landry, J.H. Perepezko, Kinetic control of silicon carbide/metal reactions, Mater. Sci. Eng., A 259 (2) (1999) 279–286.
[25] M. Kajihara, Analysis of kinetics of reactive diffusion in a hypothetical binary system, Acta Mater. 52 (5) (2004) 1193–1200.
[26] Y.-H.S.J.E. Morral, The effect of composition on marker movement and kirkendall porosity in ternary alloys, Metall. Mater. Trans. 20A (1989) 2299–2303.
[27] F.J.J. van Loo, Multiphase diffusion in binary and ternary solid-state systems, Prog. Solid State Chem. 20 (1) (1990) 47–99.
[28] V.T. Witusiewicz, A.A. Bondar, U. Hecht, T.Y. Velikanova, The Al-B-Nb-Ti system: IV. Experimental study and thermodynamic re-evaluation of the binary Al-Nb and ternary Al-Nb-Ti systems, J. Alloys Compd. 472 (1) (2009) 133–161.
[29] O. Rios, D.M. Cupid, H.J. Seifert, F. Ebrahimi, Characterization of the invariant reaction involving the L, η, γ and σ phases in the Ti-Al-Nb system, Acta Mater. 57 (20) (2009) 6243–6250.
[30] Z. Shi, H. Wei, H. Zhang, T. Jin, X. Sun, Q. Zheng, The role of Kirkendall porosity in determining β→δ transformation types in Nb-Ti-Al alloys, Int. J. Refract. Metals Hard Mater. 60 (2016) 108–112.
[31] D.M. Shah, D.L. Anton, Evaluation of refractory intermetallics with A15 structure for high temperature structural applications, Mater. Sci. Eng., A 153 (1) (1992) 402–409.
[32] P. Tsakiropoulos, Beyond Nickel Based Superalloys, 2010.
[33] K. Zelenitsas, P. Tsakiropoulos, Study of the role of Al and Cr additions in the microstructure of Nb-Ti-Si in situ composites, Intermetallics 13 (10) (2005) 1079–1095.
[34] N. Vellios, P. Tsakiropoulos, The role of Fe and Ti additions in the microstructure of Nb-18Si-5Sn silicide-based alloys, Intermetallics 15 (12) (2007) 1529–1537.
[35] H. Springer, A. Kostka, E.J. Payton, D. Raabe, A. Kaysser-Pyzalla, G. Eggeler, On the formation and growth of intermetallic phases during interdiffusion between low-carbon steel and aluminum alloys, Acta Mater. 59 (4) (2011) 1586–1600.
[36] T. Oğurtani, Kinetics of diffusion in the Nb-Al system, Metall. Mater. Trans. B 3 (2) (1972) 425–429.
[37] N. Wang, C. Du, J. Hou, Y. Zhang, K. Huang, S. Jiao, H. Zhu, Direct synthesis of Nb-Al intermetallic nanoparticles by sodiothermic homogeneous reduction in molten salts, Intermetallics 43 (2013) 45–52.
[38] X. Lei, X. Wang, F. Kong, Y. Chen, The high temperature wetting and corrosion mechanism analysis of Nb by TiAl alloy melt, Corrosion Sci. (2021), 109316.
[39] V.I. Dybkov, Reaction diffusion in heterogeneous binary systems, J. Mater. Sci. 21 (9) (1986) 3078–3084.
[40] S. Hanada, Y. Murayama, Y. Abe, High-temperature deformation of Nb3Al alloys, Intermetallics 2 (3) (1994) 155–165.
[41] C.E. Lundin, A.S. Yamamoto, EQUILIBRIUM PHASE DIAGRAM, NIOBIUM (COLUMBIUM)-ALUMINUM, 1966.
[42] L. Kokot, R. Horyn, N. Iliew, The niobium-aluminium binary system phase equilibria at 1100 °C and superconductivity of alloys, J. Less Common Met. 44 (1976) 215–219.
[43] J.L. Jorda, R. Flükiger, A. Junod, J. Muller, Metallurgy and superconductivity in Nb-Al, magnetics, IEEE Transactions on 17 (1981) 557–560.
[44] Y. Abe, S. Hanada, S. Saito, K. Hirano, N. Kobayashi, Compositions at Nb_3Al Phase boundaries at 1873K in the Nb-Al binary phase diagram, Scripta Metall. Mater. 32 (1) (1995) 27–30.
[45] C. He, F. Stein, M. Palm, Thermodynamic description of the systems Co-Nb, Al-Nb and Co-Al-Nb, J. Alloys Compd. 637 (2015) 361–375.
[46] U. Gosele, K. Tu, Growth kinetics of planar binary diffusion couples: "Thin-film case" versus "bulk cases, J. Appl. Phys. 53 (1982) 3252–3260.
[47] J. Geng, P. Tsakiropoulos, A study of the microstructures and oxidation of Nb-Si-Cr-Al-Mo in situ composites alloyed with Ti, Hf and Sn, Intermetallics 15 (3) (2007) 382–395.
[48] G. Slama, A. Vignes, Diffusion dans les aluminiures de niobium, J. Less Common Met. 29 (2) (1972) 189–202.
[49] J.L. Jorda, R. Flükiger, J. Muller, A New metallurgical investigation of the niobium-aluminium system, J. Less Common Met. 75 (2) (1980) 227–239.
[50] P. George, S.C. Parida, R.G. Reddy, Thermodynamic studies on the system Nb-Al, Metall. Mater. Trans. B 38 (1) (2007) 85–91.